# Correlation between Inactive Cathepsin D Expression and Retinal Changes in *mcd2/mcd2* Transgenic Mice

*Dan Zhang,*[1,2] *Meliha Brankov,*[1,2] *Mahindra T. Makhija,*[3] *Terry Robertson,*[4] *Erik Helmerhorst,*[3] *John M. Papadimitriou,*[4] *and Piroska E. Rakoczy*[1,2]

**Purpose.** To investigate the correlation between the presence of the inactive cathepsin D (CatD) and retinal changes in *mcd2/mcd2* transgenic mice.

**Methods.** Computational modeling was used to examine whether CatD mutants maintain competitive substrate binding. D407 cells were transfected with pcDNACatDM1 or pcDNA-CatDM2, containing procathepsin D (pro-CatD) with 6-bp (CatDM1) or 12-bp (CatDM2) deletions, respectively, flanking the pro-CatD cleavage site, and the aspartic protease activity of the transfected cells was measured. Subsequently, transgenic mice (*mcd2/mcd2*) containing CatDM2 were generated. Relative transgene copy number and transcript levels in the previously produced *mcd/mcd* (carrying CatDM1) and *mcd2/mcd2* mice were measured by quantitative real-time PCR. Western blot analysis and aspartic protease activity were used to characterize the mutated proteins. Retinal changes were described by using color fundus photography and fluorescein angiography, histology, immunohistochemistry, and electron microscopy.

**Results.** Computational modeling of the CatDM1 and CatDM2 structures indicated that the substrate binding site was not altered. There was limited or no aspartic protease activity associated with CatDM1 and CatDM2 proteins, respectively. *Mcd2/mcd2* animals contained a higher amount of inactive CatD than *mcd/mcd* or wild-type mice. Retinal abnormalities in *mcd2/mcd2* mice developed at 3 months of age, earlier than in *mcd/mcd* mice. These changes included hypopigmentation, hyperfluorescence, retinal pigment epithelial (RPE) cell depigmentation or clumping, cell proliferation, and pleomorphism. Proliferating cells were identified as being of RPE origin.

**Conclusions.** This study demonstrated a correlation between the presence of the inactive CatD in RPE cells and the development of ophthalmoscopic, cellular, and histologic changes in the retina. (*Invest Ophthalmol Vis Sci.* 2005;46:3031–3038) DOI:10.1167/iovs.04-1510

From the [1]Department of Molecular Ophthalmology, Lions Eye Institute, Perth, Australia; the [3]Western Australian Biomedical Research Institute, School of Biomedical Sciences, Curtin University of Technology, Bentley, Australia; and the [4]Department of Pathology and [2]Centre for Ophthalmology and Visual Science, The University of Western Australia, Nedlands, Australia.

Supported by National Health and Medical Research Council of Australia Grant 981471.

Submitted for publication December 22, 2004; revised April 26, 2005; accepted July 14, 2005.

Disclosure: **D. Zhang**, None; **M. Brankov**, None; **M.T. Makhija**, None; **T. Robertson**, None; **E. Helmerhorst**, None; **J. Papadimitriou**, None; **P.E. Rakoczy**, None

The publication costs of this article were defrayed in part by page charge payment. This article must therefore be marked "*advertisement*" in accordance with 18 U.S.C. §1734 solely to indicate this fact.

Corresponding author: Piroska E. Rakoczy, The University of Western Australia Centre of Ophthalmology and Visual Sciences, Nedlands, WA, Australia; rakoczy@cyllene.uwa.edu.au.

The retinal pigment epithelium (RPE) is one of the most important cell layers in the retina, and it fulfills multiple functions. It forms a physical barrier, acts as an ionic pump, assists in amino acid and vitamin A transport, and facilitates adhesion of the neurosensory retina.[1] The melanin content of the RPE cells is responsible for the absorption of light. In addition, RPE cells have a major metabolic role.[2] They are key participants in the visual cycle, metabolizing vitamin A and converting all *trans*-retinol to 11 *cis*-retinal.[3] In addition, RPE cells are responsible for the phagocytosis and digestion of rod and cone outer segments (OS) and they contain a wide range of lysosomal enzymes that include proteases, acid phosphatases, glycosidases, arylsulfatases, acid lipase, and phospholipase.[4] RPE cells carry one of the highest phagocytic loads in the body. The effects of this large phagocytic load are further exacerbated by the fact that the RPE is made of a continuous, single layer of cells connected to each other by tight junctions,[5] thereby restricting the free passage of molecules. Taking into consideration that RPE cells are postmitotic, flattening from infancy to maturity, any changes affecting their digestive capacity, such as lysosomal enzyme activity, pH increase, and deficiency in the lysosomal pathway are destined to have a detrimental effect on retinal function. In fact, the digestion of OS is never complete, which results in the accumulation of lipofuscin in the RPE cells throughout their lives.[6,7] The synthesis of A2E, a major lipofuscin fluorophore in RPE cells, is closely associated with acidic and hydrophobic conditions within the lysosomes. A2E has been widely studied and has been linked to the development of age-related macular degeneration (AMD).[8–10] The effect of compromised lysosomal enzyme function, however, is less well understood.

One of the most important lysosomal enzymes in RPE cells is the aspartic protease cathepsin D (CatD).[11–13] CatD is a ubiquitous enzyme that is synthesized as inactive procathepsin D (pro-CatD) and is subjected to several steps of posttranslational modifications to produce the biologically active form.[14] Although ageing is generally associated with an increase in aspartic protease activity, an age-related accumulation of inactive forms of CatD or pro-CatD has been known for a long time and has recently been linked to pathologic changes.[15–18] It has been proposed that the presence of inactive forms of CatD in the RPE cells accelerates OS-derived debris accumulation thus compromising RPE function.[19] In a transgenic model carrying an inactive CatD structural analogue, RPE changes indicating accelerated debris accumulation, RPE atrophy, proliferation and the accumulation of basal laminar and linear deposits were associated with photoreceptor outer segment (POS) shortening and loss.[17] To investigate whether there is a direct correlation between the presence of inactive CatD structural analogues and retinal changes, we used computer modeling to select additional deletions at the pro-CatD cleavage site with the purpose of maintaining competitive substrate binding. Subsequently, a transgenic mouse (*mcd2/mcd2*) that carried a four-amino-acid deletion was produced. After clinical characterization, the novel *mcd2/mcd2* model and the previously described *mcd/mcd* model[17] were used to investigate the effects of inactive CatD structural homologues on the accumu-

lation of POS-derived debris and on the development of retinal abnormalities.

## Materials and Methods

### Homology Modeling of Pro-CatD and Its Two Deletion Mutants, CatDM1 and CatDM2

Because the crystallographic structure of pro-CatD is not available, a homology model of pro-CatD was prepared by fitting its primary sequence (Swiss-Prot P07339 from residue 21-412 amino acids [aa]; Swiss Prot, http://www.expasy.org/ provided in the public domain by the Swiss Institute of Bioinformatics, Geneva, Switzerland) to the available three-dimensional (3-D) structure of porcine pepsinogen (PDB accession code 3PSG),[20] which not only had the pro region preserved but had the highest sequence identity with pro-CatD. Porcine pepsinogen has been solved by x-ray crystallography at 1.65-Å resolution and shares 48% sequence identity with pro-CatD. Structural fitting was conducted using Swiss-Model (www.expasy.ch/swissmod/ Swiss Institute of Bioinformatics), which is a homology-modeling Web interface server.[21,22] Further refinements, including the search for side-chain rotamers, reconstruction of loops, and preliminary energy minimization were performed with the Swiss-PDB Viewer (SPDBV).[23] Further minimization was performed with molecular modeling software (SYBYL6.9) from Tripos Associates (St. Louis, MO).[24] The Kollman all-atom force field[25] with a 0.05 kcal/mol · Å energy gradient convergence criterion was used for minimization. The evaluation of structural parameters and prediction quality of the modeled structure was achieved using the WHATIF programs (provided in the public domain by the Biomolecular computing Resource [BimCore] Emory University, Atlanta, GA).[26,27]

The two mutants were similarly homology modeled by deleting Glu44 and Gly45 for CatDM1 and Val42, Thr43, Glu44, and Gly45 for CatDM2, by using porcine pepsinogen as a template. Both mutants were then subjected to refinement, an energy-minimization protocol as used for pro-CatD, and the quality of the structures was checked using the WHATIF programs.

### Generation of CatDM2 Mice

A plasmid containing the human CatD cDNA with a 12-nucleotide deletion in the cleavage site of CatD (pcDNACatDM2) was prepared as described previously,[28] but with the sense primer (5′-TACTCCCAGGCGGTGCCAGCC ↓ CCCATTCCCGAGGTGCTCAA-3′) containing a 12-nucleotide deletion (marked by the arrow) corresponding to nucleotides 235 to 246 of the CatD cDNA. This deletion encodes the four amino acids, valine (Val42), threonine (Thr43), glutamic acid (Glu44), and glycine (Gly45). To generate *mcd2/mcd2* transgenic mice, we microinjected the DNA construct containing the CatDM2 gene driven by the human cytomegalovirus (CMV) promoter and the polyadenylation signal from the bovine growth hormone (BGH) gene into single-cell stage C57BL/6 embryos (Transgenic Embryo Service, Walter and Eliza Hall Institute, Melbourne, Australia). Transgenic founders were identified by PCR and Southern blot analysis, as described previously.[28]

All mouse experiments were performed in accordance with the ARVO Statement for the Use of Animals in Ophthalmic and Vision Research. All mice were housed in cages at a constant temperature of 22°C, with a 12-hour light–dark cycle (lights on at 0600 hours) and food and water available ad libitum.

### Color Fundus Photography and Fluorescein Angiography (FA)

Mice were anesthetized by intraperitoneal injection of xylazine (6 mg/kg; Bayer AG, Leverkusen, Germany) and ketamine (50 mg/kg; Warner Lambert, Morris Plains, NJ) and photographed as described previously.[17]

### Genomic DNA and Total RNA Isolation

Genomic DNA of *mcd/mcd* and *mcd2/mcd2* mice was obtained from mouse tail tips (Wizard Genomic DNA Purification Kit; Promega, Madison, WI). Total RNA was extracted from retinas of enucleated eyes (RNA*later* and the RNeasy Mini Kit; Qiagen, Hilden, Germany), according to the manufacturer's instructions, with modification. Briefly, enucleated eyes were transferred into the stabilization reagent (100 μL/eye; RNA*later*; Qiagen) and placed at 4°C overnight. After dissection, the retinas were isolated from eyes, homogenized in 1 mL extraction reagent (TRIzol; Invitrogen, Carlsbad, CA), and centrifuged at 12,000*g* for 10 minutes at 4°C, to remove insoluble material. The supernatant of the homogenate was incubated at room temperature (RT) for 5 minutes and then extracted by addition of 0.2 mL chloroform with vigorous shaking for 15 seconds followed by incubation for 3 minutes at RT. After centrifugation, the upper aqueous phase was transferred to a new tube with an equal volume of isopropanol. The vortexed mixture was purified (RNeasy column; Qiagen) and washed by RW1 and RPE buffer. Total RNA was subsequently eluted into 50 μL of RNase-free water and quantified by spectrophotometry (BioPhotometer; Eppendorf, Hamburg, Germany).

### cDNA Synthesis and Real-Time PCR

For reverse transcription, total retinal RNA was subjected to cDNA synthesis (Omniscript RT Kit; Qiagen). Each reaction included 1× buffer RT, 0.5 mM of each dNTP, 1 μM Oligo-dT primer (Promega), 10 units RNase inhibitor (Promega), 4 units reverse transcriptase (Omniscript; Qiagen), and 200 ng total RNA. The cDNA was synthesized at 37°C for 1 hour and subjected to real-time PCR.

Purified genomic DNA (100 ng) or cDNA (2-μL aliquot from cDNA synthesis) was subjected to real-time PCR. Mouse glyceraldehyde-3-phosphate dehydrogenase (GAPDH) served as a normalizer for the transgene and its transcriptional product (mRNA). A transgene PCR product CD386 was used to prepare the standard curve. Concentration of the purified DNA fragment was determined using the photometer (BioPhotometer; Eppendorf), and the standard curve was composed of three 10-fold serial dilutions to give final concentrations between $10^3$ and $10^8$ gene copies. Transgene-specific primers 5′-ATGCAGCCCTCCAGCCTTCTG-3′ and 5′-GGCTGGCACCGCCTGGGAGTAC-3′ or GAPDH primers 5′-GCTGAGTATGTCGTGGAGTC-3′ and 5′-ATGGACTGTGGTCATGAGC-3′ were used in the PCR, with a final concentration of 0.2 μM each. Each reaction was conducted with 12.5 μL of master mix (Platinum SYBR Green qPCR SuperMix UDG; Invitrogen) in a final volume of 25 μL according to the manufacturer's protocol.

Reactions were performed on a commercial system (Rotor-Gene 3000; Corbett Research, Sydney, Australia) in the following conditions: holding at 50°C for 2 minutes; initial denaturation at 95°C for 2 minutes; and 45 cycles of 95°C for 15 seconds, 62°C for 30 seconds, and 72°C for 30 seconds The threshold cycle ($C_t$) was calculated with the system software (Rotor-Gene 6.0.12; Corbett Research).

### Aspartic Protease Analysis

The CatD activity of pcDNACatDM1-[28] or pcDNAM2-transfected D407 cells (a human RPE cell line from Richard Hunt, University of South Carolina, Columbia, SC) and transgenic mouse retinas was determined with hemoglobin used as a substrate,[15] with modifications. Cells or dissected retinas were homogenized in 0.5 mL lysis buffer comprising 0.1 M sodium acetate (pH 3.4) and 0.2% Triton X-100 and then incubated at room temperature for 30 minutes. Tissue debris was removed by centrifugation at 12,000*g* for 5 minutes. Recovered supernatant (50 μL), in triplicate, was serially diluted into a 96-well plate, with addition of 50 μL of 2% hemoglobin in 0.1 M sodium acetate (pH 3.4) to each well. The reaction was incubated at 37°C for 1 hour followed by protein precipitation by the addition of 50 μL ice-cold 10% trichloroacetic acid. The samples were incubated overnight at 4°C before centrifugation at 250*g* for 10 minutes. The supernatants, containing released peptides from the digested hemoglobin, were measured with a protein assay kit (MicroBCA; Pierce, Rockford, IL). The resultant

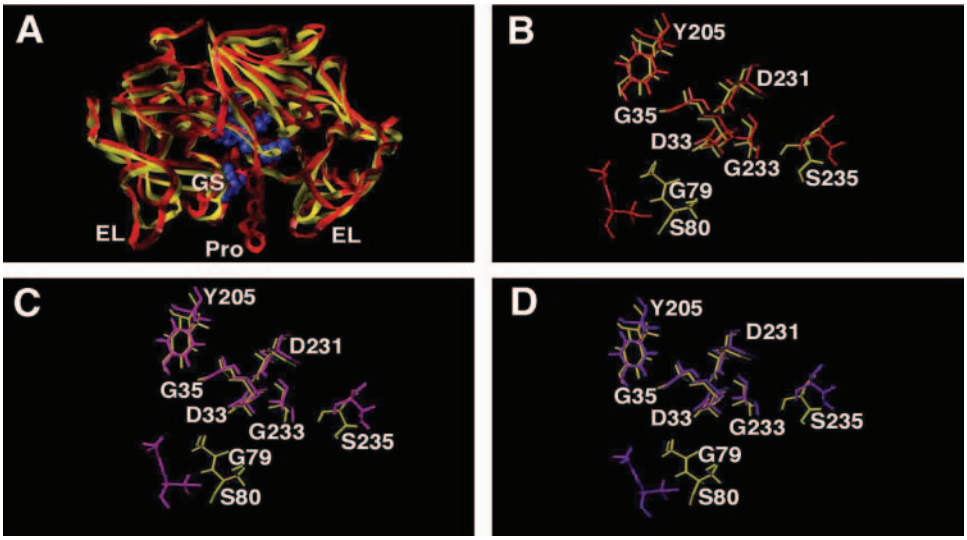


**FIGURE 1.** CatD superimposed on models of pro-CatD and its mutants. (**A**) Homology model of pro-CatD (*red*) is superimposed on the crystallographic structure of CatD (*yellow*) with active site residues in *blue*. EL, extended loop regions; Pro, pro region of pro-CatD; GS, Gly79 to Ser80 of the active site. (**B–D**) Active site amino acid residues of CatD (*yellow*) are labeled and superimposed on the active site of the model of pro-CatD (*red*; **B**) and the deletion mutants CatDM1 (*magenta*; **C**), and CatDM2 (*purple*; **D**).

bicinchoninic acid (BCA) complex was measured at 570 nm with an automatic ELISA reader (Dynatech Medical; linked to BioLinx 2.10 software; Dynatech Laboratories, Cambridge, MA). Standard curves were established with bovine cathepsin (Sigma-Aldrich, St. Louis, MO).

### Western Blot Analysis

Retinal protein samples were prepared for analysis of aspartic protease activity in 0.1 M sodium acetate (pH 3.4) lysis buffer. The pH was then adjusted to 7.0 in loading buffer for Western blot analysis. CatD was detected with a monoclonal CatD antibody (Ab-1; Oncogene Research Products, Boston, MA) followed by a sheep anti-mouse IgG-horseradish peroxidase (HRP) secondary antibody (GE Healthcare, Buckinghamshire, UK). The chemiluminescence was then measured with Western blot detection reagents (ECL Plus; GE Healthcare).

### Histology, Immunohistochemistry, and Electron Microscopy

All mice were euthanized at 3 ($n$ = 7), 6 ($n$ = 8), and 12 ($n$ = 8) months of age with an overdose of sodium pentobarbital. The eyes were enucleated and fixed for 4 hours in 10% neutral buffered saline or 4% paraformaldehyde. After routine processing through a graded alcohol series, the eyes were embedded in paraffin and sectioned at 5 $\mu$m, mounted on silanated slides, and stained with hematoxylin and eosin (H&E). For immunohistochemistry, paraffin-embedded sections were deparaffinized, rehydrated, and bleached, to remove melanin by incubation of sections in 0.25% potassium permanganate for 20 minutes and in 1% oxalic acid for 5 minutes before incubation with anti-proliferating cell nuclear antigen (PCNA; DakoCytomation, Glostrup, Denmark) or rabbit anti-human RPE65 (a gift from T. Micheal Redmond, National Eye Institute, Bethesda, MD). Correspondingly, the secondary antibodies were goat anti-mouse IgG alkaline phosphatase conjugate (Chemicon, Temecula, CA) or goat anti-rabbit IgG AP conjugate (Chemicon) followed by detection with alkaline phosphatase substrate (Fast Red; Sigma-Aldrich). Sections were counterstained with Mayer's hematoxylin for light microscopy. Preparation of tissue and transmission electron microscopy were performed as described earlier.[17]

## RESULTS

### Computer Analysis of the 3-D Structures and Comparison of Aspartic Protease Activity of the Inactive CatD Structural Analogues

Computation modeling of CatDM1 and CatDM2 was undertaken to predict whether the mutations were likely to alter the conformation of residues comprising the substrate binding sites of the proteins relative to CatD. Pro-CatD and two deletion mutants (CatDM1 and CatDM2) were homology modeled by using the crystallographic structure of pepsinogen. Pepsinogen was chosen for the homology modeling, because it shares a high degree of amino acid identity with pro-CatD and the equivalent pro region in pro-CatD is preserved in pepsinogen. Furthermore, the crystallographic structure of pepsinogen was solved at high resolution (1.65 Å), thereby giving confidence in the prediction of the homology-modeled structures. The root mean square $z$-values (RMS-Z) were calculated by the WHATIF program, describing bond lengths, angles, torsions, and improper dihedral angles, and the results indicated that the quality of each model developed was satisfactory. There were some steric clashes of side chains observed in each of the computed models. However, these clashes were relieved after further minimization of each structure. A high level of confidence in the quality of the models was also afforded after the superpositioning of the peptide backbone of the homology-modeled pro-CatD on the known crystallographic structure of CatD (Fig. 1A). An excellent closeness of fit was observed except, as was expected, in some of the extended loop regions. The pro region in pro-CatD was observed extending down between the extended loop regions and was juxtapositioned adjacent to the active site residues of CatD. The active-site amino acid residues of CatD were essentially superpositioned with the equivalent residues in pro-CatD and each of the two mutants (Figs. 1B–D). No significant differences were observed in the positioning of any of the active site residues in either pro-CatD or the CatDM1 and CatDM2 mutants. The slight displacement of Gly79-Ser80 residues in pro-CatD and CatDM1 and CatDM2 mutants was not unexpected, because these residues are located as part of a mobile loop region on the surface of the protein. These comparisons suggest that it is unlikely that the mutations in CatDM1 and CatDM2 alter the substrate binding properties of the mutant proteins relative to pro-CatD and CatD.

Plasmid constructs, including a 12-bp deletion corresponding to the Val42, Thr43, Glu44, and Gly45 amino acids flanking the pro-CatD cleavage site (pcDNACatDM2), a plasmid of CatDM1 (pcDNACatDM1),[28] a negative control (pcDNA), and a normal CatD gene (pcDNACatD) were transfected into D407 cells (Fig. 2A). There was no statistically significant increase in aspartic protease activity in stably transfected cells when enzymatic activity was compared between native D407 (114 ± 17 U/mg protein) and pcDNA (98 ± 16 U/mg protein) transfected cells. Aspartic protease activity increased fourfold in

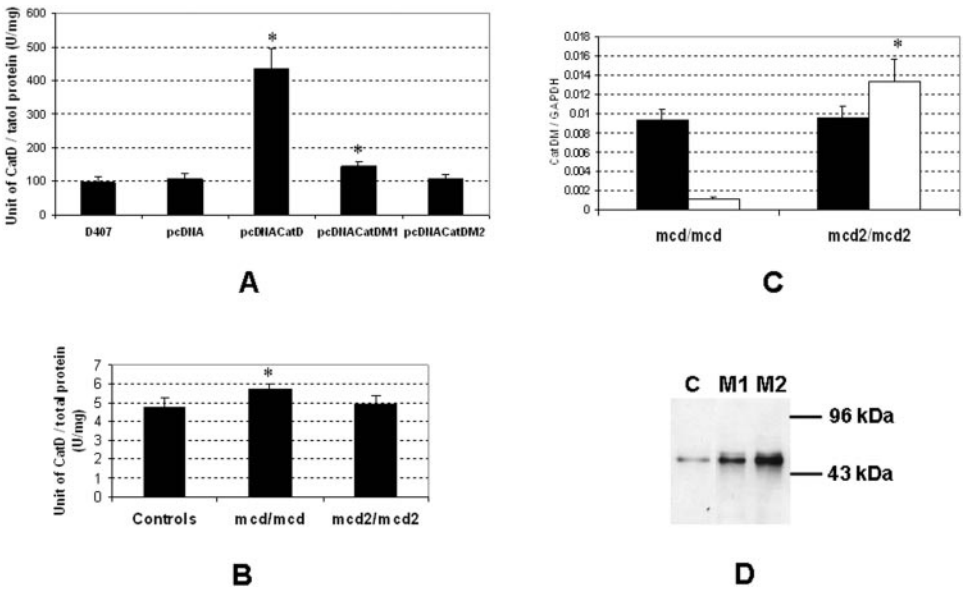


**FIGURE 2.** Molecular characterization of the mutated CatD gene and its product in D407 cells and transgenic mouse retinas. (**A**) Aspartic proteinase activity assay of D407 cells transfected with the plasmid DNA constructs pcDNA, pcDNACatD, pcDNACatDM1, and pcDNACatDM2. D407 is a control of nontransfected D407 cells. $^*P <$ 0.05 compared with D407. (**B**) Aspartic proteinase activity assay of retinas of *mcd/mcd* ($n = 3$) and *mcd2/mcd2* ($n = 3$) mice, and C57BL/6 control mice ($n = 3$). $^*P \leq 0.05$ compared with the control. (**C**) Real-time PCR quantification of the transgene and the transcript copies in *mcd/mcd* and *mcd2/mcd2* mice. (■) Gene quantification performed with genomic DNA of *mcd/mcd* ($n = 5$) and *mcd2/mcd2* ($n = 5$) mice and plotted as DNA copies of the transgene normalized to DNA copies of mouse GAPDH gene. (□) Real-time RT-PCR for quantification of the transgene cDNA derived from mRNA of *mcd/mcd* ($n = 3$) and *mcd2/mcd2* ($n = 3$) mice. The quantification is plotted as mRNA copies of the transgene normalized to mRNA copies of the mouse GAPDH gene. The approaches in (**C**) are determined from the CD386 DNA standard curve. $^*P < 0.001$ compared with *mcd/mcd.* (**D**) Western blot analysis of transgene expression in the retinas of *mcd/mcd* (M1) and *mcd2/mcd2* (M2), showing the dominant CatD band. C, C57BL/6 control.

pcDNACatD (422 ± 58 U/mg protein) transfected cells when compared with native D407 cells. There was a small but statistically significant increase in aspartic protease activity in pcDNACatDM1 (143 ± 14 U/mg protein; $P < 0.05$) transfected cells, but enzymatic activity remained unchanged in pcDNACatDM2-transfected cells (105 ± 11 U/mg protein, $P \geq 0.2$) when compared with the control native D407 cells (Fig. 2A). These results demonstrate that CatDM2 is unable to produce biologically active CatD. The aspartic protease activity measured in the eyes of the different groups of mice is presented in Figure 2B. Compared with control C56BL/6 mouse eyes (4.7 ± 0.5 U/mg total protein), there was a significant but slight increase in aspartic protease activity in *mcd/mcd* eyes (5.7 ± 0.4 U/mg protein; $P \leq 0.05$), but not in *mcd2/mcd2* mouse eyes (4.9 ± 0.5 U/mg protein; $P \geq 0.4$).

## Molecular Comparison of *mcd/mcd* and *mcd2/mcd2* Mice

Southern blot analysis and PCR amplification confirmed the generation of three founders of *mcd2/mcd2* mice. From the three founders one stable homozygous transgenic line (*mcd2/mcd2*) was established and used for the studies described herein.

The *mcd/mcd*[17] and *mcd2/mcd2* lines carried the same copy number of the integrated transgene in their genomes ($P \geq 0.1$; Fig. 2C). However, the amount of mutated CatD transcript was 12-fold higher in *mcd2/mcd2* than in *mcd/mcd* ($P < 0.001$) mouse retinas (Fig. 2C). The presence of a higher copy number of transcripts in *mcd2/mcd2* mice translated into elevated CatD immunoreactivity corresponding to a higher amount of mutated CatD protein in the *mcd2/mcd2* eyes when compared with *mcd/mcd* and wild-type mouse eyes (Fig. 2D). Considering that, in wild-type mice, the amount of endogenous CatD does not vary significantly (Vagaja N, Zhang D, unpublished results, 2003), the increase in immunoreactivity in the *mcd/mcd* and *mcd2/mcd2* mice must be attributable to higher transgene expression in *mcd/mcd* and *mcd2/mcd2* (Fig. 2C).

Because of the presence of impaired cleavage sites, aspartic protease activity was not expected to increase in *mcd/mcd* and *mcd2/mcd2* eyes when compared with C57BL/6 eyes. There was, however, a lower but significant increase in aspartic protease activity in *mcd/mcd* mice when compared with the control animals. However, the presence of a large amount of mcd2/mcd2 protein was not accompanied by any statistically significant increase in aspartic protease activity. Hence, these data indicate that the presence of an elevated amount of the mutated CatD in the *mcd2/mcd2* mice did not result in an increase in aspartic protease activity when compared with *mcd/mcd* or wild-type control mice.

## Clinical and Histologic Evaluation of *mcd2/mcd2* Mice

Clinical examination (color fundus photography and FA) of C57Bl/6J mice revealed no changes in the appearance of the retinas between 3, 6, and 12 months of age. In *mcd2/mcd2* mice ($n = 18$), the fundus appeared normal up to 3 months of age (Fig. 3A). At the age of 3 months, ophthalmic examination showed clinical changes in 67% (24/36) of *mcd2/mcd2* eyes. Single (18/36; Fig. 3B) or geographic (6/36; Fig. 3C) hypopigmentary changes were present, primarily in the superior lateral quadrant. At 6 and 12 months of age, 75% (12/16) and 87.5% (14/16) of examined eyes, respectively, showed areas of hypopigmentation. Hyperpigmentation was rarely observed in *mcd2/mcd2* mice. FA showed the presence of discrete hyperfluorescence in the regions corresponding to hypopigmentation (Figs. 4A, 4B). The area showing hypopigmentary changes and hyperfluorescence gradually increased with age (Fig. 4B, arrow). A modest increase in the intensity of hyperfluorescence was observed between the early and late phases of FA, at both 6 (Figs. 4C, 4E, arrowheads) and 12 (Figs. 4D, 4F, arrowheads) months of age, but there was no increase in the size of the hyperfluorescent areas. The appearance of hyperfluorescence was unlike the signal generated by leaky blood vessels and no pooling was present.

Light microscopy of 3- and 12-month-old *mcd2/mcd2* eyes demonstrated gradual morphologic changes in RPE cells and the photoreceptor layer. The morphology of 3-month-old *mcd2/mcd2* retinas remained normal in most parts of the retina (Fig. 5A). However, there were localized regions where RPE cells were disorganized, clumped, and in some instances

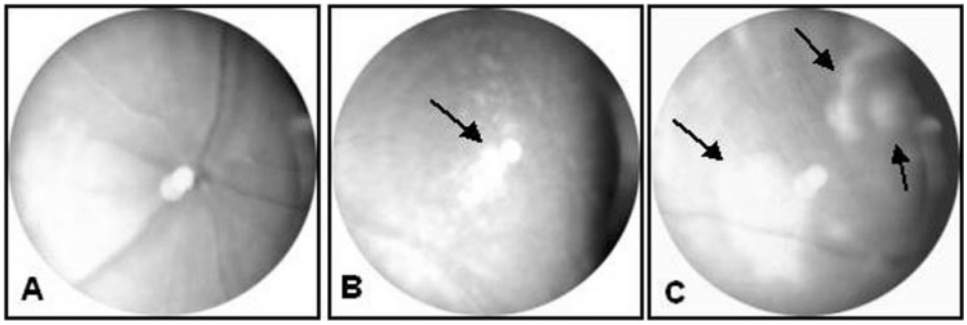


**FIGURE 3.** Color fundus photography of typical *mcd2/mcd2* mouse retinas at 3 months of age showed (**A**) normal fundus with no pigmentary changes; (**B**) a hypopigmentary region (*arrow*), primarily in the superior lateral quadrant; (**C**) more widespread depigmentation and a geographic pattern (*arrows*).

proliferating (Fig. 5B, arrows). In addition, pleomorphism of RPE cells (Fig. 5C, thick arrows) and some degenerative changes in the outer nuclear layer (ONL; Fig. 5C, thin arrows) such as a decrease in the number of rows of nuclei was present. In the retinas of 12-month-old animals, there were also localized regions in which pigmented RPE cells appeared to be absent (Fig. 5D, arrows). These regions usually included RPE attenuation with depigmentation and atrophy (Fig. 5E, thick arrows), but Bruch's membrane remained intact irrespective of age (Fig. 5E, thin arrows). These RPE changes are often described as "pigment mottling" or RPE attenuation with depigmentation, hypertrophy, hyperplasia, and/or atrophy. Whenever pigment mottling was noted, the adjacent POS layer showed disturbances (Figs. 5B, 5C, 5E). Progressive loss of photoreceptors (Fig. 5F; black asterisks) by 12 months was combined with the subsequent localized thinning of ONL (Fig. 5F, white asterisks). The earliest features of pigment mottling in *mcd2/mcd2* mice appeared at 3 months of age, showing RPE cell proliferation (79%), RPE depigmentation (50%), and RPE pleomorphism (42%; Table 1). The prevalence of histologically evident changes in the RPE layer increased over time, and, by 12 months of age, 94% of the animals demonstrated RPE proliferation. The severity of the changes also increased with age with RPE detachment and loss of photoreceptors observed in 6- and 12-month-old *mcd2/mcd2* mice (Table 1).

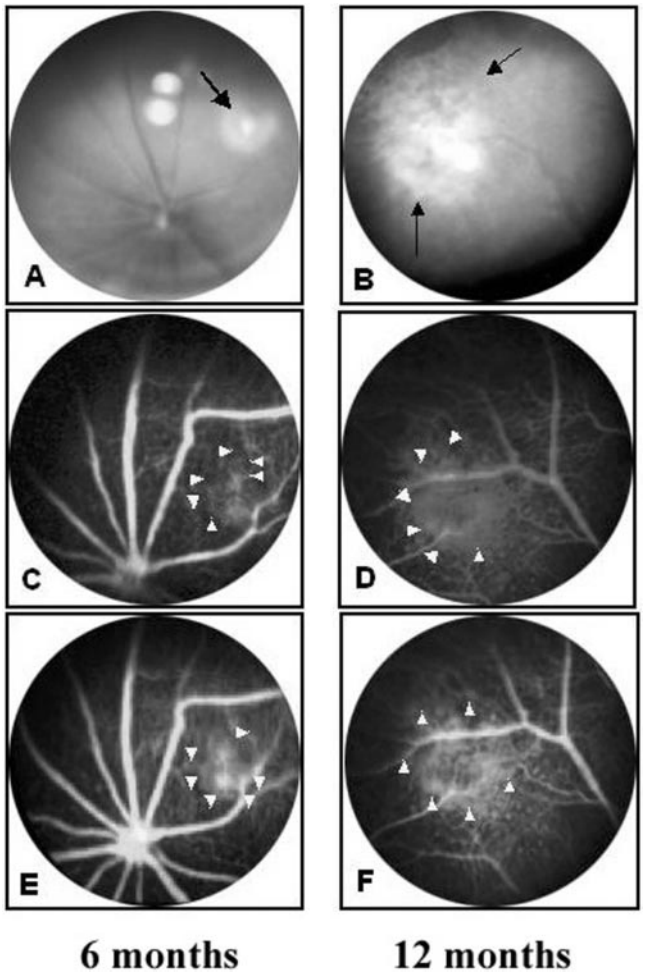


**FIGURE 4.** Color fundus photography and FA of a typical *mcd2/mcd2* mouse retina at (**A**) 6 months demonstrated a hypopigmentary region (*arrow*) and at (**B**) 12 months showed that areas of hypopigmentary changes had increased with age (*arrows*). FA at 6 (**C**) and at 12 (**D**) months in an early phase revealed an area of discrete hyperfluorescence (*arrowheads*), due to abnormal fluorescence of the choriocapillaris as a result of RPE atrophy (**E**) and (**F**). The surface of the fluorescing zone remained constant in the late phase of FA, but the intensity of the fluorescence increased rapidly (*arrowheads*).

## Immunohistochemical and Electron Microscopic Analysis

One of the features of *mcd2/mcd2* mice was the appearance of unusual pigmented cells in the subretinal space immediately subjacent to the RPE layer (Figs. 5G–I). To investigate the precise nature and source of these cells, immunohistochemistry was performed, with a CD68 antibody used to detect macrophages, a MOMA-2 antibody to detect newly recruited monocytes, an RPE65 antibody to detect RPE cells, a PCNA antibody to detect proliferating cells, and tomato lectin staining to identify glial cells. There was no positive immunostaining with CD68, MOMA-2, or tomato lectin, confirming that the proliferating cells in the subretinal space were not macrophages, monocytes or glial cells (data not shown). Positive immunostaining was detected with a polyclonal RPE65 antibody and a monoclonal PCNA antibody (Figs. 5H, 5I, respectively), indicating that the unusual pigmented cells were proliferating cells and were most likely to be of RPE cell origin. As expected, the proliferating cells of the subretinal space did not stain with tomato lectin, although occasional cells in the ganglion layer were stained, indicating the presence of cells of the inner nuclear layer (data not shown).

Electron microscopic examination of retinas with proliferating cells identified two morphologic types of RPE cells: relatively thin, poorly pigmented cells (Fig. 6, asterisks) which retained their position directly adjacent to Bruch's membrane and relatively large but heavily pigmented daughter cells that were situated within the layer of rods and cones, often resting on the original RPE layer (Figs. 5G, 6, large arrow). Invariably, the often poorly pigmented RPE cells displayed almost complete loss of pigment granules and some reduction in the secretory granule producing machinery (Golgi complex, endoplasmic reticulum). The morphology of mitochondria and other cytoplasmic organelles did not display abnormalities, but

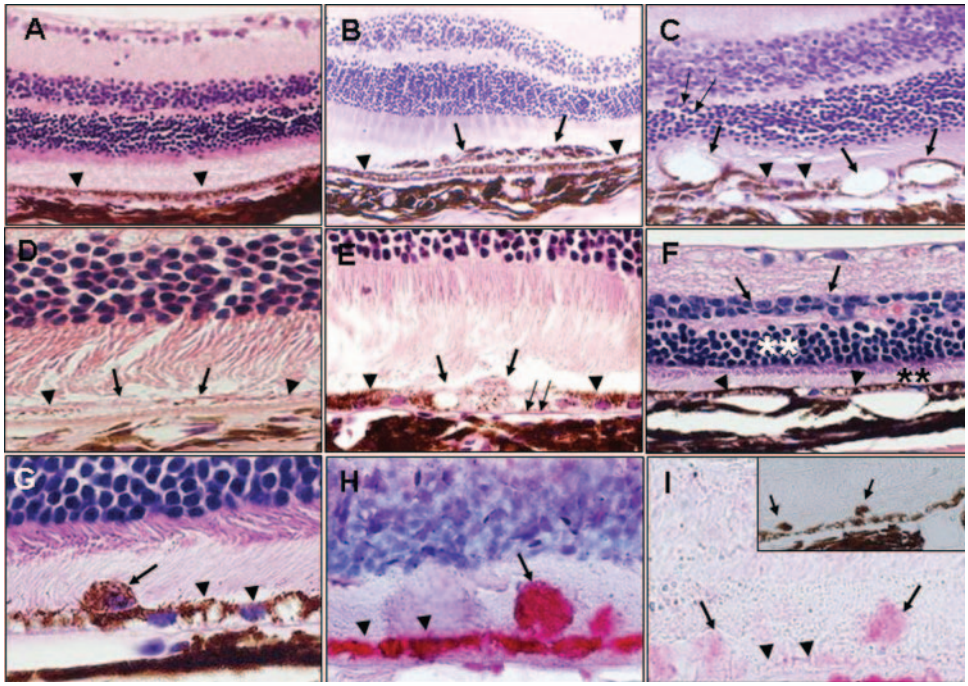


**FIGURE 5.** Histology and immunohistochemistry of *mcd2/mcd2* retinas. H&E-stained retinal sections of (**A–C**) 3- and (**D–F**) 12-month-old *mcd2/mcd2* mice. (**G–I**) Immunohistochemistry of the unusual pigmented giant cells in 12-month-old *mcd2/mcd2* retinas. (**A**) The morphology of the retina remained normal in most areas. (**B**) A retinal section showing abnormal hyperproliferation of RPE cells (*arrows*). (**C**) Retina of a *mcd2/mcd2* mouse with pleomorphic RPE cells (*thick arrows*) and degenerative changes in the outer nuclear layer (*thin arrows*). (**D**) The morphology of *mcd2/mcd2* retina demonstrated widespread depigmented regions where RPE cells were totally absent (*arrows*). (**E**) RPE cell changes, often described as pigment mottling, appeared as RPE attenuation with depigmentation and atrophy (*thick arrows*), but with Bruch's membrane remaining intact (*thin arrows*). (**F**) Retina of a *mcd2/mcd2* mouse showing progressive shortening of the outer segment layer (*black asterisks*), a decrease in rows of photoreceptor nuclei (*white asterisks*), and thinning of the inner nuclear layer (*arrows*). (**G**) An H&E–stained section demonstrating a giant cell located above the RPE cell layer (*arrow*). (**H**) RPE cells on a bleached retinal section were detected by labeling with anti-RPE65. (**I**) Labeling of giant cells with anti-PCNA on bleached retinal sections was confirmed by their appearance on unbleached sequential control section (*inset*). *Arrowheads*: RPE cell layer in each image.

phagosomes were generally few. Junctional complexes were retained, although endocytic contents containing remains of rods and cones were reduced. The basal lamina appeared unaffected. All these suggest that these poorly pigmented cells remained viable for some time. In contrast, proliferating daughter cells demonstrated abnormal cytoarchitectural features (Fig. 6, larger arrow). Apart from their large size, the nuclei were often not basally polarized (Fig. 6, N) and there was almost complete loss of tight junctions. However, these cells displayed many melanosomes and several phagosomes. In addition, evidence of endocytosis of rod and cone OS was present at multiple sites along the cell periphery (Fig. 6, small arrows).

## DISCUSSION

In this work, an increase in the amount of CatD structural analogues resistant to proteolysis did not elevate endogenous aspartic protease activity but initiated morphologic, cellular, and functional changes in the RPE cells. Owing to its degradative role, CatD is tightly regulated, to ensure that it functions only when needed. CatD is produced as pro-CatD, which is subjected to a series of posttranslational modifications. The main process of proteolytic maturation of pro-CatD is through the action of lysosomal cysteine proteases,[29,30] via the removal of the propeptide.[31,32] The fact that the removal of two or four amino acids adjacent to the cleavage site was sufficient to impair the activation process suggests that a highly specific process of proteolytic cleavage for the pro-CatD maturation and consequently activation was abolished.[14]

The *mcd/mcd* (CatDM1) and *mcd2/mcd2* (CatDM2) transgenic mice retained their fully functional endogenous CatD. The presence of CatDM1 and CatDM2 proteins in the RPE cells is thought to compromise the lysosomal digestion of OS by competitive binding of the substrate. Comparison of the known 3-D structure of CatD with homology models of pro-CatD, CatDM1, and CatDM2 suggests that the architecture of the active site was not altered by the mutations used in this study. The only predicted changes in conformation were confined to amino residues in some of the extended loop regions of the proteins. The mobility and uncertainty of amino acid residues in these loop regions is often high and is not unexpected. In conclusion, the computer modeling suggests that the residue-binding sites in CatDM1 and CatDM2 proteins are unchanged and would compete with native CatD for substrate binding. After the generation of the substrate/CatD complexes, only substrate bound to endogenous, biologically active CatD is subjected to proteolysis.

Although the genome of *mcd/mcd* and *mcd2/mcd2* mice contained the same copy numbers of their respective transgenes and carried the same promoter, transcription and translation were more efficient in the *mcd2/mcd2* mice. Consider-

**TABLE 1.** Summary of the Histological Analysis of *mcd2/mcd2* Mice at the Ages of 3, 6, and 12 Months

| Age (mos) | Eyes (*n*) | RPE Proliferation | RPE Depigmentation | RPE Pleomorphism | RPE Detachment | Loss of Photoreceptor Cells |
|---|---|---|---|---|---|---|
| 3 | 14 | 11/14 (79) | 7/14 (50) | 6/14 (42) | 0/14 (0) | 0/14 (0) |
| 6 | 16 | 14/16 (88) | 9/16 (56) | 8/16 (50) | 3/16 (19) | 8/16 (50) |
| 12 | 16 | 15/16 (94) | 11/16 (69) | 10/16 (63) | 6/16 (38) | 14/16 (88) |

Data are the number of eyes examined in the age group, with the percentage affected shown in parentheses.

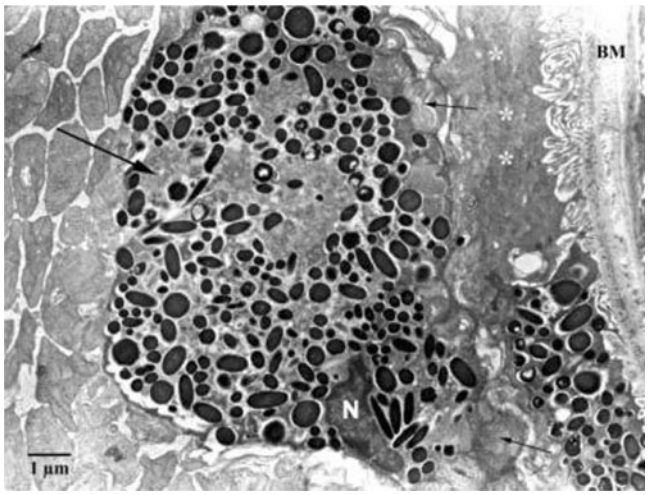


**FIGURE 6.** A transmission electron micrograph of RPE cells in a 1.5-year-old *mcd2/mcd2* transgenic mouse. Two different types of RPE cells were observed directly adjacent to Bruch's membrane. One was heavily pigmented, whereas the other was a relatively thin, nonpigmented cell (*white asterisks*). A proliferating RPE daughter cell (*large arrow*) was located adjacent to the RPE cells resting on Bruch's membrane (BM). This cell contained a nonbasal nucleus (N), many melanosomes, several phagosomes, and evidence of endocytosis of rods and cones at multiple sites along the cell surface (*small arrows*).

ing that both transgenic mouse lines were produced by the same process of random integration, the higher level of transgene production in the *mcd2/mcd2* mice is probably due to the site of integration. In addition, CatDM2 protein may have an increased stability compared with CatDM1 and endogenous pro-CatD.

The accumulation of lipofuscin, which is an indigestible product of phagocytosis in the brain and in the RPE cells, is one of the hallmarks of aging.[33,34] Excessive presence of lipofuscin has been linked to functional abnormalities.[35–38] Generally, the presence of breakdown products in phagocytosing cells is thought to compromise the normal function of these cells and both mouse lines demonstrated the accumulation of POS-derived debris in the RPE cells. Considering the presence of a more inactive CatD structural analogue in *mcd2/mcd2* mice, an accelerated accumulation of photoreceptor-derived breakdown products in the RPE cells and the earlier functional failure of these cells were expected. Indeed, when compared with the *mcd/mcd* mice, *mcd2/mcd2* animals exhibited abnormal depigmented regions in the retina at 3 months of age, which is well ahead of the appearance of the same disease phenotype at 10 to 12 months of age in the *mcd/mcd* animals.[17] With time, the area affected by depigmentation gradually increased, and the retina became increasingly abnormal and the ophthalmoscopic appearance of the eyes resembled geographic atrophy in humans. Histology confirmed that the changes started with RPE cell proliferation. Over the course of 1 year, the number of photoreceptors gradually decreased. However, the progress toward the development of the disease phenotype remained slow. In clinical and morphologic phenotypes, *mcd2/mcd2* mice were generally similar to *mcd/mcd*. Considering the presence of early RPE changes in large areas of the retina at 3 months of age, the delayed development of the disease phenotype was surprising.

Closer examination of the proliferating cells in the *mcd2/mcd2* mice not only confirmed that these cells were proliferating RPE cells, but revealed a significant difference between the parent and daughter cells. Unusual pigmented giant cells have been shown in the retinal section of collagen XVIII/endostatin–deficient aged mice,[39] but the origin of these cells was different from the cells observed in the aged *mcd2/mcd2* mice. In the collagen XVIII/endostatin–deficient aged mice, the giant cells originated from the iris stroma, were located above the ganglion cell layer, and had macrophage-like characteristics. Proliferating cells in the *mcd2/mcd2* mice were located in the subretinal region, and immunohistochemistry confirmed not only their RPE origin, but also their proliferating nature. It appears that in *mcd2/mcd2* mice the mutation is associated with the reduction or absence of the melanosomes observed as poorly pigmented RPE cells, and with phagocytic performance, as judged from the paucity of lysosomes and phagosomes, which may lead to local injury in adjoining tissues with subsequent reparative attempts by the RPE cells at these sites.[40] Regenerative attempts, however, appear to be disorganized, with daughter RPE cells detaching from Bruch's membrane and from each other, enlarging in size and becoming heavily melanized. Although endocytosis appears structurally unaffected, loss of normal architectural relationships may further contribute to the local injury. We suggest that the initiation of proliferation of postmitotic RPE cells may play a role in delaying the development of the full disease phenotype in the *mcd/mcd* and *mcd2/mcd2* mouse models.

The correlation between the development of disease phenotypes and the presence of mutations has been one of the basic axioms of genetic research. A mutation can cause a wide range of changes, resulting in the lack of a gene product, in the production of a truncated protein, or in an undesirable conformational alteration.[41–43] Recently, there has been an explosion in the number of genetically linked diseases and, with the completion of the human genome project, these numbers are set to further increase. However, the case–cause relationship between a genetic mutation and a disease phenotype is not always easy to establish, particularly not in the case of complex diseases. Several complex diseases such as type II diabetes, AMD, and some forms of cancer have been associated with aging.[44–46] In these conditions, genetic mutations represent only a predisposition that acts with dietary, behavioral, and environmental effects in unison, resulting in the development of a particular disease phenotype.

We propose that *mcd/mcd* and *mcd2/mcd2* transgenic models are an example of how the presence of a mutation might represent a predisposition to a condition without development of the full disease phenotype. Further studies to examine the effect of a variety of genetic, behavioral, and environmental effects on the development of the AMD phenotype are necessary, to establish the significance of these factors in AMD development, not only in the *mcd/mcd* and *mcd2/mcd2* models, but also in humans.

## *Acknowledgments*

The authors thank May C. Lai for technical assistance and comments on the manuscript.

## *References*

1. Bok D. The retinal pigment epithelium: a versatile partner in vision. *J Cell Sci Suppl*. 1993;17:189–195.
2. Sarna T. Properties and function of the ocular melanin: a photobiophysical view. *J Photochem Photobiol B*. 1992;12:215–258.
3. Redmond TM, Yu S, Lee E, et al. Rpe65 is necessary for production of 11-cis-vitamin A in the retinal visual cycle. *Nat Genet*. 1998;20:344–351.
4. Eldred GE. *The Retinal Pigment Epithelium.* New York: Oxford University Press; 1998;653–654.
5. Hudspeth AJ, Yee AG. The intercellular junctional complexes of retinal pigment epithelia. *Invest Ophthalmol*. 1973;12:354–365.

6. Young RW. Shedding of discs from rod outer segments in the rhesus monkey. *J Ultrastruct Res*. 1971;34:190–203.
7. Spitznas M, Hogan MJ. Outer segments of photoreceptors and the retinal pigment epithelium: interrelationship in the human eye. *Arch Ophthalmol*. 1970;84:810–819.
8. Shaban H, Richter C. A2E and blue light in the retina: the paradigm of age-related macular degeneration. *Biol Chem*. 2002;383:537–545.
9. Sparrow JR, Parish CA, Hashimoto M, Nakanishi K. A2E, a lipofuscin fluorophore, in human retinal pigmented epithelial cells in culture. *Invest Ophthalmol Vis Sci*. 1999;40:2988–2995.
10. Ben-Shabat S, Parish CA, Hashimoto M, et al. Fluorescent pigments of the retinal pigment epithelium and age-related macular degeneration. *Bioorg Med Chem Lett*. 2001;11:1533–1540.
11. Rakoczy PE, Lai CM, Baines M, et al. Modulation of cathepsin D activity in retinal pigment epithelial cells. *Biochem J*. 1997;324:935–940.
12. Regan CM, de Grip WJ, Daemen FJ, Bonting SL. Degradation of rhodopsin by a lysosomal fraction of retinal pigment epithelium: biochemical aspects of the visual process. XLI. *Exp Eye Res*. 1980;30:183–191.
13. Bosch E, Horwitz J, Bok D. Phagocytosis of outer segments by retinal pigment epithelium: phagosome-lysosome interaction. *J Histochem Cytochem*. 1993;41:253–263.
14. Davies DR. The structure and function of the aspartic proteinases. *Annu Rev Biophys Biophys Chem*. 1990;19:189–215.
15. Boulton M, Moriarty P, Jarvis-Evans J, Marcyniuk B. Regional variation and age-related changes of lysosomal enzymes in the human retinal pigment epithelium. *Br J Ophthalmol*. 1994;78:125–129.
16. Wiederanders B, Oelke B. Accumulation of inactive cathepsin D in old rats. *Mech Ageing Dev*. 1984;24:265–271.
17. Rakoczy PE, Zhang D, Robertson T, et al. Progressive age-related changes similar to age-related macular degeneration in a transgenic mouse model. *Am J Pathol*. 2002;161:1515–1524.
18. Wilcox DK. Vectorial accumulation of cathepsin D in retinal pigmented epithelium: effects of age. *Invest Ophthalmol Vis Sci*. 1988;29:1205–1212.
19. Rakoczy PE, Baines M, Kennedy CJ, Constable IJ. Correlation between autofluorescent debris accumulation and the presence of partially processed forms of cathepsin D in cultured retinal pigment epithelial cells challenged with rod outer segments. *Exp Eye Res*. 1996;63:159–167.
20. Hartsuck JA, Koelsch G, Remington SJ. The high-resolution crystal structure of porcine pepsinogen. *Proteins*. 1992;13:1–25.
21. Schwede T, Kopp J, Guex N, Peitsch MC. SWISS-MODEL: An automated protein homology-modeling server. *Nucleic Acids Res*. 2003;31:3381–3385.
22. Guex N, Peitsch MC. SWISS-MODEL and the Swiss-PdbViewer: an environment for comparative protein modelling. *Electrophoresis*. 1997;18:2714–2723.
23. Peitsch MC. Protein modelling by E-mail. *Biotechnology*. 1995;13:658–660.
24. *SYBYL Molecular Modelling System.* St. Louis: Tripos, Inc.
25. Singh UC, Kollman PA. An approach to computing electrostatic charges for molecules. *J Comput Chem*. 1984;5:129–145.
26. Vriend GJ. WHATIF: a molecular modelling and drug design program. *J Mol Graph*. 1990;8:52–56.
27. Hooft RW, Vriend G, Sander C, Abola EE. Errors in protein structures. *Nature*. 1996;381:272.
28. Zhang D, Lai MC, Constable IJ, Rakoczy PE. A model for a blinding eye disease of the aged. *Biogerontology*. 2002;3:61–66.
29. Gieselmann V, Hasilik A, von Figura K. Processing of human cathepsin D in lysosomes in vitro. *J Biol Chem*. 1985;260:3215–3220.
30. Samarel AM, Ferguson AG, Decker RS, Lesch M. Effects of cysteine protease inhibitors on rabbit cathepsin D maturation. *Am J Physiol*. 1989;257:C1069–C1079.
31. Erickson AH. Biosynthesis of lysosomal endopeptidases. *J Cell Biochem*. 1989;40:31–41.
32. Faust PL, Kornfeld S, Chirgwin JM. Cloning and sequence analysis of cDNA for human cathepsin D. *Proc Natl Acad Sci USA*. 1985;82:4910–4914.
33. Mrak RE, Griffin ST, Graham DI. Aging-associated changes in human brain. *J Neuropathol Exp Neurol*. 1997;56:1269–1275.
34. Boulton M, Dayhaw-Barker P. The role of the retinal pigment epithelium: topographical variation and ageing changes. *Eye*. 2001;15:384–389.
35. Davies S, Elliott MH, Floor E, et al. Photocytotoxicity of lipofuscin in human retinal pigment epithelial cells. *Free Radic Biol Med*. 2001;31:256–265.
36. Finnemann SC, Leung LW, Rodriguez-Boulan E. The lipofuscin component A2E selectively inhibits phagolysosomal degradation of photoreceptor phospholipid by the retinal pigment epithelium. *Proc Natl Acad Sci USA*. 2002;99:3842–3847.
37. Shamsi FA, Boulton M. Inhibition of RPE lysosomal and antioxidant activity by the age pigment lipofuscin. *Invest Ophthalmol Vis Sci*. 2001;42:3041–3046.
38. Katz ML, Redmond TM. Effect of Rpe65 knockout on accumulation of lipofuscin fluorophores in the retinal pigment epithelium. *Invest Ophthalmol Vis Sci*. 2001;42:3023–3030.
39. Marneros AG, Olsen BR. Age-dependent iris abnormalities in collagen XVIII/endostatin deficient mice with similarities to human pigment dispersion syndrome. *Invest Ophthalmol Vis Sci*. 2003;44:2367–2372.
40. Hiscott P, Sheridan C, Magee RM, Grierson I. Matrix and the retinal pigment epithelium in proliferative retinal disease. *Prog Retin Eye Res*. 1999;18:167–190.
41. Wang Q, Chen Q, Zhao K, et al. Update on the molecular genetics of retinitis pigmentosa. *Ophthalmic Genet*. 2001;22:133–154.
42. Fauser S, Luberichs J, Schuttauf F. Genetic animal models for retinal degeneration. *Surv Ophthalmol*. 2002;47:357–367.
43. Cremers FP, van den Hurk JA, den Hollander AI. Molecular genetics of Leber congenital amaurosis. *Hum Mol Genet*. 2002;11:1169–1176.
44. Tchernof A, Labrie F. Dehydroepiandrosterone, obesity and cardiovascular disease risk: a review of human studies. *Eur J Endocrinol*. 2004;151:1–14.
45. Meneilly GS. Pathophysiology of type 2 diabetes in the elderly. *Clin Geriatr Med*. 1999;15:239–253.
46. Zarbin MA. Current concepts in the pathogenesis of age-related macular degeneration. *Arch Ophthalmol*. 2004;122:598–614.